View metadata, citation and similar papers at core.ac.uk

brought to you by CORE

provided by Elsevier - Publisher Connector

Biophysical Journal Volume 79 August 2000 1129–1138

Sensitivity Enhancement in Fluorescence Correlation Spectroscopy of Multiple Species Using Time-Gated Detection

Don C. Lamb,* Andreas Schenk,† Carlheinz Röcker,† C. Scalfi-Happ,† and G. Ulrich Nienhaus*,†

*Department of Physics, University of Illinois at Urbana-Champaign, Urbana, Illinois 61801-3080 USA; and †Department of Biophysics, University of Ulm, D-89069 Ulm, Germany

ABSTRACT Fluorescence correlation spectroscopy (FCS) is a powerful technique to measure chemical reaction rates and diffusion coefficients of molecules in thermal equilibrium. The capabilities of FCS can be enhanced by measuring the energy, polarization, or delay time between absorption and emission of the collected fluorescence photons in addition to their arrival times. This information can be used to change the relative intensities of multiple fluorescent species in FCS measurements and, thus, the amplitude of the intensity autocorrelation function. Here we demonstrate this strategy using lifetime gating in FCS experiments. Using pulsed laser excitation and laser-synchronized gating in the detection channel, we suppress photons emitted within a certain time interval after excitation. Three applications of the gating technique are presented: suppression of background fluorescence, simplification of FCS reaction studies, and investigation of lifetime heterogeneity of fluorescently labeled biomolecules. The usefulness of this technique for measuring forward and backward rates of protein fluctuations in equilibrium and for distinguishing between static and dynamic heterogeneity makes it a promising tool in the investigation of chemical reactions and conformational fluctuations in biomolecules.

INTRODUCTION

In recent years, fluctuation correlation spectroscopy (FCS) has become a prominent technique in the fields of chemistry, biochemistry, and biophysics (Eigen and Rigler, 1994; Maiti et al., 1997). The method has single-molecule sensitivity and can be used with fluorophore concentrations in the nanomolar to femtomolar range. Solution FCS studies typically measure intensity fluctuations of the light emitted by fluorophores in a subfemtoliter open volume. The small sample volume is created by tight focusing of a laser beam using high numerical aperture objectives and confocal detection or two-photon excitation. The fluctuations in fluorescence intensity may arise from various sources, such as translational diffusion of molecules in and out of the probe volume (Magde et al., 1974), rotational diffusion within the probe volume (Ehrenberg and Rigler, 1974; Aragón and Pecora, 1976; Kask et al., 1989), triplet state excitation (Widengren et al., 1994, 1995), chemical reactions (Magde et al., 1974, 1976; Rauer et al., 1996), and conformational fluctuations (Bonnet et al., 1998; Haupts et al., 1998).

Whenever a fluorescent molecule diffuses into the detection volume, it will be excited, and fluorescence emission will be registered until it exits again. Thus, photons do not arrive purely stochastically in time at the detector, but come in bursts. The more slowly the molecule diffuses, the longer such bursts will last on the average. If the fluorescent molecule undergoes a chemical reaction, its diffusion coefficient may change by, e.g., association with another molecule, which will also affect the duration of the bursts. Moreover, the reaction may also affect the intensity or spectral shape of the emitted fluorescence, and thus the intensity measured by the detector within its spectral bandwidth may flicker during a burst due to repeated forward and backward reaction steps.

FCS is a particular example of a class of experiments that measure thermodynamic fluctuations of an observable as a function of time or frequency. In an FCS experiment, fluorescence quanta and their respective arrival times are collected from many bursts, and the observed fluorescence fluctuations are quantified by statistical methods such as photon counting histogram analysis (Chen et al., 1999; Kask et al., 1999) or correlation functions (Palmer and Thompson, 1989; Thompson, 1991). Here we will be concerned with the latter approach. In the intensity autocorrelation function (ACF), the amplitude depends on the average number of fluorescent particles in the volume and hence on the concentration, whereas the correlation times provide information about the time scales of the intensity fluctuations. Each registered photon, however, carries more information than its arrival time relative to that of other photons. It has a particular energy, polarization, and delay time between absorption and emission. This additional information can be used to enhance the sensitivity of FCS to a particular fluorescent species.

Here we discuss the weighting of the ACF based on the relative intensity of the individual components. We use a pulsed laser as the excitation source and a laser-synchronized gate in the detection channel. This method allows us to vary the relative contributions of species having different fluorescence lifetimes to the ACF, which is useful in a variety of applications, such as rejection of background fluorescence, increase in sensitivity towards a particular fluorescent species, and the study of lifetime distributions, which are frequently observed in the fluorescence emission of biological macromolecules.

Received for publication 14 January 2000 and in final form 17 May 2000.

Address correspondence to Gerd Ulrich Nienhaus, Universitaet Ulm, Abt. Biophysik, Albert-Einstein-Allee 11, 89081 Ulm, Germany. Tel.: 49-731-502-3050; Fax: 49-731-502-3059; E-mail: uli@uiuc.edu.

© 2000 by the Biophysical Society

0006-3495/00/08/1129/10 $2.00

MATERIALS AND METHODS

FCS setup

For the experiments reported here, we used an FCS setup with pulsed two-photon excitation, in which two near-infrared photons are absorbed simultaneously to induce an electronic transition in the visible (Göppert-Mayer, 1931). It consists of an argon-ion laser pumped Ti:Sapphire laser (Mira 900; Coherent, Palo Alto, CA), producing 150-fs pulses at 76 MHz and 790 nm, and an epi-illuminated fluorescence microscope (Axiovert 135 TV; Carl Zeiss, Jena, Germany). The light was focused into the sample by a water-immersion objective (C-Apochromat, 63 × NA 1.2, Zeiss). The resulting fluorescence was collected through the same objective, separated from the laser light by a dichroic mirror (640DCXPSR; Chroma Technology, Brattleboro, VT) and filter (BG 39; Schott, Mainz, Germany) and focused onto an avalanche photodiode detector (APD model SPCM-AQ-161; EG&G Optoelectronics Canada, Vaudreuil, Canada) operated in single photon counting mode. The APD output was connected to a correlator card (model 5000/E, ALV, Langen, Germany) through a fast transistor–transistor logic (TTL) AND gate. The output from a silicon semiconductor diode consisting of positively doped, not doped (intrinsic), negatively doped material photodiode (FND 100 Q, EG&G Optoelectronics Canada), which was illuminated by a fraction of the laser light, was used as a trigger for generating a gate pulse (with adjustable delay and width) that was applied to one of the AND gate inputs. The TTL output of the APD was compressed to 2 ns and connected to the other input. Consequently, APD pulses were only propagated through the gate when the gating signal level was high. The delay of the gate was adjusted to begin suppressing photons coincident with the laser pulse and was not varied during the experiments reported here.

Fluorescence intensity decays were measured using a computer card for time-correlated single photon counting (TimeHarp 100, PicoQuant, Berlin, Germany). These data were least-squares fitted with multiple exponentials, which were convoluted with the instrument function determined independently.

Sample preparation

All chemicals, unless stated otherwise, were analytical grade and dissolved in MilliQ water (Millipore, MilliQ Plus). Tetramethylrhodamine (TMR) and 1-anilino-8-naphthalene sulfonic acid (ANS) were purchased from Molecular Probes (Eugene, OR). For the ANS binding studies, horse heart apomyoglobin was purchased from Sigma-Aldrich (St. Louis, MO), dissolved in 10 mM potassium phosphate buffer, pH 7.0, centrifuged for 15 min at 2,800 *g* at room temperature to remove any aggregates or impurities, and diluted to a concentration of 300 nM. A small amount of ANS solution was added directly to the 300 nM apomyoglobin sample in 10 mM potassium phosphate buffer (pH 7.0) to give a final ANS concentration of 1 μM. For reference measurements of protein diffusion in the absence of ANS ligands, myoglobin was stochastically labeled with Oregon Green (Oregon Green 514 carboxylic acid succinimidyl ester, Molecular Probes) according to standard procedures.

For the FCS experiments with fluorescently labeled sperm whale myoglobin, the protein was extracted from sperm whale skeletal muscle using the method described by Antonini and Brunori (1971). The resulting myoglobin precipitate was dialyzed repeatedly, further purified using column chromatography, and freeze-dried until needed. Sperm whale metmyoglobin, which includes the heme group in the oxidized form, was labeled with 5-carboxy-tetramethylrhodamine succinimidyl ester (TAMRA-SE; Molecular Probes), which binds randomly to the ϵ-amino group of one of 19 lysines or the amino terminus of the polypeptide chain. The degree of labeling was determined photometrically as 0.66, using the extinction coefficients $\epsilon_{409} = 157\ \mathrm{mM^{-1}\ cm^{-1}}$ for metmyoglobin and $\epsilon_{554} = 85\ \mathrm{mM^{-1}\ cm^{-1}}$ for TMR. To obtain labeled apomyoglobin, the heme group was extracted according to the procedure of Teale (1959). The sample was subsequently reacted with TAMRA-SE, yielding a degree of labeling of 0.30, based on the extinction coefficients of $\epsilon_{280} = 32.6\ \mathrm{mM^{-1}\ cm^{-1}}$ and $\epsilon_{554} = 85\ \mathrm{mM^{-1}\ cm^{-1}}$ for TMR and $\epsilon_{280} = 14.75\ \mathrm{mM^{-1}\ cm^{-1}}$ for apomyoglobin.

To bind the fluorescent label at a specific site, we used the sperm whale myoglobin mutant E109C, which has the glutamic acid residue 109 replaced by cysteine. The plasmid for this mutant was a kind gift from Prof. Steve Sligar (UIUC). The mutant protein was expressed in *Escherichia coli* and purified as described (Springer and Sligar, 1987). Tetramethylrhodamine-5-maleimide (Molecular Probes) was conjugated to the thiol group of C109, and a labeling degree of 0.99 was determined photometrically. For specifically labeled apomyoglobin, the heme group was removed from labeled metmyoglobin E109C protein (Teale, 1959). The amount of labeled apomyoglobin, determined photometrically, was also above 99%. Matrix-assisted laser desorption ionization time-of-flight mass spectroscopy (MALDI-TOF-MS) measurements were performed on apomyoglobin samples to verify the identity and purity of the reactants.

AUTOCORRELATION ANALYSIS

We present here a brief overview of the theoretical background of FCS, focusing on the case of two-photon excitation of multiple fluorescent species. For reviews of the mathematical details, we refer the reader to Elson and Magde (1974), Aragón and Pecora (1976), and Thompson (1991). Autocorrelation analysis yields the correlation times of the intensity fluctuations in FCS experiments. The observed fluorescence intensity is given by the sum over all fluorescent species,

$$F(t) = \frac{1}{2}\sum_{j=1}^{n} \kappa_j \sigma_j Q_j \int d\mathbf{r} W(\mathbf{r}) C_j(\mathbf{r}, t). \qquad (1)$$

Here, κ_j is the detection efficiency of species j, which depends on the spectral response of the detection system to the fluorescence emission, σ_j is the two-photon absorption cross section at the wavelength of excitation, and Q_j is the fluorescence quantum yield. Thus the product $\kappa_j\ \sigma_j\ Q_j$ is a measure for the photon collection yield of a particular species j. The concentration, $C_j\ (\mathbf{r}, t)$, is a function of both space and time because of the dynamic processes present in the sample (e.g., diffusion or chemical reactions). $W(\mathbf{r})$ denotes the product of the squared excitation intensity distribution, the extent of the sample, and the emission intensity distribution measured at the detector and thus quantifies the spatial variation in the yield of photons from the excitation volume. We refer to $\int d\mathbf{r} W(\mathbf{r})$ as the probe volume.

The fluorescence intensity fluctuates in time, and correlations in the fluctuations can be uncovered by calculating the normalized intensity ACF, $G(\tau)$, defined as

$$G(\tau) = \frac{\langle F(t)F(t+\tau)\rangle - \langle F(t)\rangle^2}{\langle F(t)\rangle^2}, \qquad (2)$$

where $\langle\ \rangle$ denotes the time average.

In one-photon confocal spectroscopy and two-photon spectroscopy, the function $W(\mathbf{r})$ is often treated as a three-dimensional Gaussian. For pure diffusion of n non-interact-

ing species in a three-dimensional Gaussian probe volume with radial dimension w_r and axial dimension w_z (denoting the distance from the center at which the intensity has decayed by a factor of e^2), $G(\tau)$ can be calculated analytically from Eqs. 1 and 2 and is given by

$$G(\tau) = \sum_{j=1}^{n} \Im_j^2 G_{D_j(\tau, N_j, \tau_{D_j})}, \quad (3)$$

which is the sum over the diffusion ACFs of all species j, G_{D_j},

$$G_{D_j}(\tau, N_j, \tau_{D_j}) = \frac{\gamma}{\langle N_j \rangle} \left(\frac{1}{1 + \tau/\tau_{D_j}} \right) \left(\frac{1}{1 + (w_r/w_z)^2 \tau/\tau_{D_j}} \right)^{1/2}, \quad (4)$$

weighted by the square of the fractional intensity contribution of species j, $\Im_j$,

$$\Im_j = \frac{\kappa_j \sigma_j Q_j \langle C_j \rangle}{\sum_{k=1}^{n} \kappa_k \sigma_k Q_k \langle C_k \rangle}. \quad (5)$$

In Eq. 4, $\gamma = (1/2)^{3/2}$ is a normalization factor, and $\langle N_j \rangle$ is the average number of molecules of type j in the probe volume. The diffusion time, τ_{D_j}, is given by

$$\tau_{D_j} = \frac{w_r^2}{4D_j} \quad \text{or} \quad \tau_{D_j} = \frac{w_r^2}{8D_j} \quad (6)$$

for one- or two-photon excitation, respectively, where D_j is the diffusion coefficient of species j.

In the presence of chemical reactions, the species can interconvert, and the spatio-temporal fluctuations of the concentrations, $C_j(\mathbf{r}, t)$, are governed by the reaction-diffusion differential equation,

$$\frac{\partial}{\partial t} C_j(\mathbf{r}, t) = D_j \nabla^2 C_j(\mathbf{r}, t) + \sum_{k=1}^{n} T_{jk} C_k(\mathbf{r}, t), \quad (7)$$

where T_{jk} is a matrix of the kinetic coefficients, and n includes all species involved in the reaction (although they may not be fluorescent). Even for two interacting species, Eq. 7 has no general closed-form solution. For the discussion that follows we will consider two particular cases: a unimolecular reaction, where each state has the same diffusion coefficient, and a bimolecular reaction, where one of the reactants has the same diffusion coefficient as the product and the other reactant is in excess (pseudo-first order; Elson and Magde, 1974; Aragón and Pecora, 1976; Thompson, 1991).

Unimolecular reaction

For a unimolecular reaction,

$$A \underset{k_b}{\overset{k_f}{\rightleftharpoons}} B, \quad (8)$$

A and B represent the two interconverting species; k_f and k_b are the forward and backward reaction rates. The concentration of each component is given by the solution of the matrix equation

$$\frac{\partial}{\partial t} \begin{pmatrix} C_A(\mathbf{r}, t) \\ C_B(\mathbf{r}, t) \end{pmatrix} = \begin{pmatrix} D_A \nabla^2 - k_f & k_b \\ k_f & D_B \nabla^2 - k_b \end{pmatrix} \begin{pmatrix} C_A(\mathbf{r}, t) \\ C_B(\mathbf{r}, t) \end{pmatrix}. \quad (9)$$

When both states have the same diffusion coefficient, $D_A = D_B = D$, the mathematics simplifies and the ACF can be obtained in closed form,

$$G(\tau) = G_D(\tau, N_A + N_B, \tau_D) \left[1 + K \left(\Im_A - \frac{\Im_B}{K} \right)^2 e^{-\lambda \tau} \right], \quad (10)$$

where $K = k_f/k_b$ is the equilibrium coefficient, and $\lambda = k_f + k_b$ is the apparent reaction rate coefficient. The presence of a reaction appears as a relaxation term in the ACF. This term will disappear for $\Im_A = \Im_B/K$, and thus, according to Eq. 5, when the photon collection yields, $\kappa_A \sigma_A Q_A$ and $\kappa_B \sigma_B Q_B$, are equal. This reflects the trivial fact that number fluctuations of the two species can only be observed if they affect the overall photon emission. Note that the relaxation term is maximized when only one of the two states emits fluorescence photons and has its largest amplitude when this state occurs less frequently than the dark state.

If the diffusion coefficients of the two species are not identical, a closed-form ACF can also be obtained, but only for the special case that the reaction occurs on a much faster time scale than the difference of the diffusion times of the two species through the probe volume. This equation is given in the Appendix.

Bimolecular Reaction

For the bimolecular reaction of a macromolecule M with a ligand L,

$$M + L \underset{k_b}{\overset{k_f}{\rightleftharpoons}} ML, \quad (11)$$

the set of differential equations governing the concentrations is given by

$$\frac{\partial}{\partial t} \begin{pmatrix} C_M(\mathbf{r}, t) \\ C_L(\mathbf{r}, t) \\ C_{ML}(\mathbf{r}, t) \end{pmatrix} = \begin{pmatrix} D_M \nabla^2 - k_f \langle C_L \rangle & -k_f \langle C_M \rangle & k_b \\ -k_f \langle C_L \rangle & D_L \nabla^2 - k_f \langle C_M \rangle & k_b \\ k_f \langle C_L \rangle & k_f \langle C_M \rangle & D_{ML} \nabla^2 - k_b \end{pmatrix} \cdot \begin{pmatrix} C_M(\mathbf{r}, t) \\ C_L(\mathbf{r}, t) \\ C_{ML}(\mathbf{r}, t) \end{pmatrix}. \quad (12)$$

Here we will consider the reaction of small ligands with a macromolecule, so that changes in the diffusion coefficient

upon ligand binding can be neglected, and hence $D_M = D_{ML} = D$. Moreover, if we assume pseudo-first-order conditions with an abundance of ligand, $\langle C_L \rangle \gg \langle C_M \rangle$, the ACF can be calculated without any further approximations and is given by

$$G(\tau) = G_D(\tau, N_M + N_{ML}, \tau_D) \cdot \left[(\Im_M + \Im_{ML})^2 + K\langle C_L \rangle \left(\Im_M - \frac{\Im_{ML}}{K\langle C_L \rangle} \right)^2 e^{-\lambda\tau} \right] + G_D(\tau, N_L, \tau_{D_L}) \Im_L^2. \quad (13)$$

Here, $K = k_f/k_b$ is the equilibrium coefficient, and $\lambda = k_f(\langle C_M \rangle + \langle C_L \rangle) + k_b$ is the apparent rate coefficient of the reaction. Again, the reaction appears as a relaxation term in the ACF. Note that the equation is not symmetric with respect to ligands and macromolecules because of their different diffusion coefficients.

As shown in the Appendix, a closed-form expression of the ACF can also be obtained if the reaction is much faster than ligand diffusion through the probe volume. If the reaction is much slower than ligand diffusion through the volume, the reacting species can be treated as non-interacting particles (Eq. 3). For slow, irreversible reactions, progress of the reaction can be followed by measuring the amplitude of the ACF as a function of time (Schwille et al., 1997; Kettling et al., 1998).

APPLICATIONS OF LIFETIME-GATED DETECTION IN FCS EXPERIMENTS

Suppression of background fluorescence

In FCS experiments, there are always unwanted fluorescent impurities in the sample. Under certain conditions (for instance when measuring *in vivo*), a high background is unavoidable. In this situation, it can be beneficial to discriminate between fluorophores based on their different excited-state lifetimes. This can be done by exciting the sample with laser pulses and excluding detected photons with a certain time delay between excitation and emission from the data analysis. Lifetime gating changes the relative intensities of fluorescent species with different lifetimes and, hence, their contribution to the ACF. The correlation function measured with and without the gate can also give information about the diffusion coefficient, and hence the size, of the impurity. Measuring the amplitude of the ACF as a function of the gate pulse width and performing a global analysis yields the population of each species, provided that their lifetimes differ markedly.

Here we demonstrate the effectiveness of the gating technique for measurements in a sample with background fluorescence using a mixture of 10 nM TMR and 25 μM ANS, so that each species has a similar fluorescence intensity. The lifetime of TMR is 2.2 ns, whereas the lifetime of ANS in aqueous buffer is <100 ps (Bismuto et al., 1996). In Fig. 1, ACFs obtained from this mixture are shown for various gate widths. For comparison, we also show the ACF of a 10 nM TMR sample without ANS. In the latter case, we obtain a simple diffusion ACF, characterized by a correlation time $\tau_D = 32 \pm 1$ μs and a fluctuation amplitude of 0.36, reflecting the fact that, according to Eq. 4, one molecule resided in our probe volume on average. By adding ANS to the solution, more molecules are in the probe volume, on average, and consequently, the fluctuation amplitude decreases. Note that $G(0)$ drops by only a factor of ~2, although the number of molecules increases about 2500-fold. This is a consequence of the fact that, according to Eq. 3, the relative contributions are weighted by the square of the fractional intensities, and ANS has a much smaller absorption and lower quantum yield than TMR. Since the number of ANS molecules is three orders of magnitude larger than the number of TMR molecules, the diffusion autocorrelation term of the ANS molecules can be neglected, and Eq. 3 reduces to

$$G(\tau) = (\Im_{TMR})^2 G_{Diff}(\tau, N_{TMR}, \tau_{D_{TMR}}). \quad (14)$$

By suppressing the fluorescence within the first 300 ps after the excitation pulse, the correlation amplitude increases to 0.23, indicating that the background fluorescence from the ANS contributes less to the measured ACF. As we increase the gate width, the correlation curve approaches the one of the TMR-only sample, and with an effective gate width of 1.4 ns, $G(\tau)$ of TMR with ANS is virtually indistinguishable from that of TMR alone. Time-gated FCS increases the correlation amplitude and hence the signal level by suppressing photons from *both* the target species and the background fluorophores. Therefore, a remark about the signal-to-noise ratio (S/N) of the measured ACF is in order. Two limiting cases can be distinguished (Koppel, 1974). In the high count rate limit, the average number of photons per

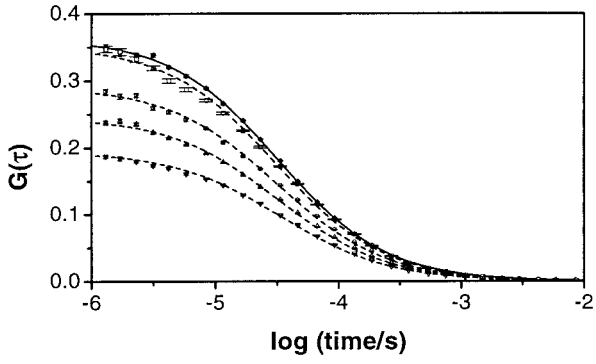

FIGURE 1 Fluorescence intensity autocorrelation data and fits with Eqs. 3 and 4 of 10 nM TMR (*full symbols* and *solid line*) and a dye mixture of 10 nM TMR and 25 μM ANS at three different gate settings (*open symbols* and *dashed lines,* from bottom to top: no gate/0.3 ns/0.9 ns/1.4 ns), plotted versus the logarithm of time in seconds.

sampling interval is large, and the uncertainty in the ACF is dominated by the stochastic nature of the intensity fluctuations. In this case, the loss of photons from time gating will not affect the noise level as long as the high count rate limit is maintained. In the low count rate limit, the average number of photons per sampling interval is small, and the uncertainty is governed by photon shot noise. In this case, the S/N at early times is proportional to $I_T \cdot G(0)$, where I_T is the average overall count rate (Koppel, 1974). The gate width can be chosen to either provide the optimum S/N or to obtain the correct $G(0)$ value. Fig. 2 is a plot of the calculated I_T, $G(0)$, and S/N for a mixture of TMR and ANS of equal intensity as a function of the gate width. For these two dyes, the best S/N occurs for a gate width of 300 ps. It obviously increases most if the lifetimes of the dyes are markedly different, because the short lifetime components can be suppressed with minimal effect on the long lifetime component. Hence, probes with long excited-state lifetimes can be used very effectively in FCS with gated detection.

Ligand binding studies

Quantitatively accurate values of the forward and backward reaction rate coefficients of chemical reactions can be obtained from solution FCS experiments. Lifetime gating can also be extremely beneficial for this kind of application. As an example, we take the reaction of ANS binding to apomyoglobin. ANS in solution is only weakly fluorescent, but its fluorescence increases by more than a factor of 100 when it binds to the hydrophobic heme pocket of the protein. Concomitantly, the fluorescence lifetime increases enormously (Stryer, 1965). Fig. 3 *b* shows the fluorescence intensity of ANS in water and in a solution of apomyoglobin as a function of the delay from the excitation pulse. Whereas the intensity decay of free ANS is very fast and limited by the intrinsic time response of our detection system, the protein-bound ANS shows a much slower decay with a lifetime of 12.4 ± 0.2 ns. This pronounced sensitivity of ANS to its environment makes it an excellent probe for studies of protein stability and dynamics (Bismuto et al., 1993, 1996; Sirangelo et al., 1998).

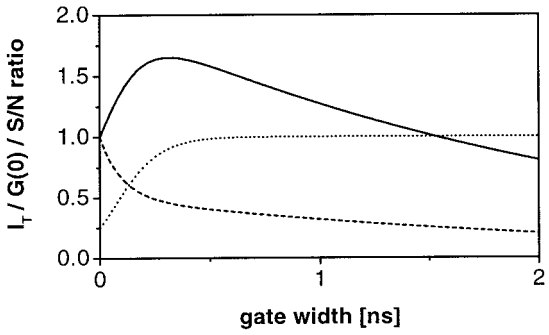

FIGURE 2 Change in fluorescence intensity, I_T (*dashed line*), $G(0)$ (*dotted line*), and S/N (*solid line*) of the ACF in the low count rate limit, calculated for a sample containing TMR ($\tau_F = 2.2$ ns) in an ANS ($\tau_F = 0.1$ ns) background of equal fluorescence intensity as a function of gate width.

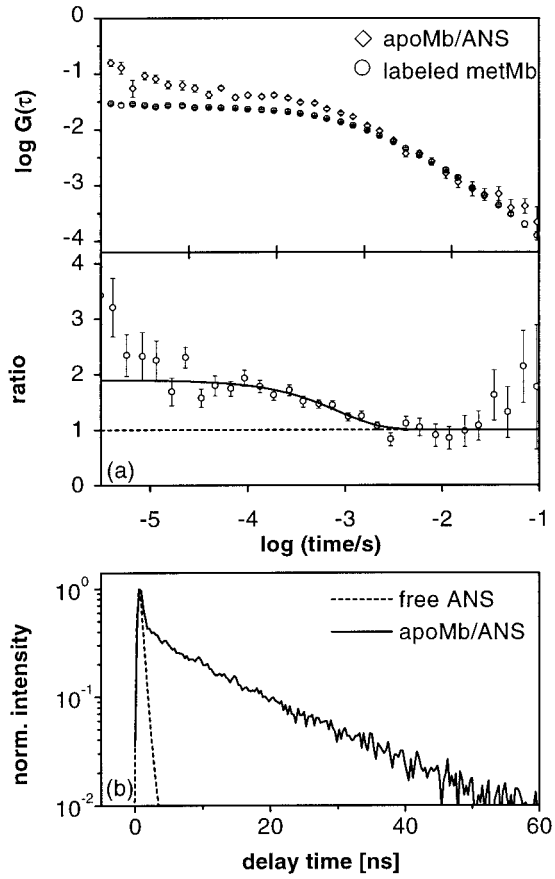

FIGURE 3 (*a*) Double-logarithmic plot of the intensity ACFs of apomyoglobin in the presence of 1 μM ANS, taken with the gate set at 2 ns to suppress the fluorescence contribution from free ANS, and of fluorescently labeled Mb. The former ACF was scaled to compensate for the difference in protein concentration between the two samples. The ratio of the above ACFs is shown in the lower panel. The solid line is a fit with $1 + e^{-\lambda\tau}/(K\langle C_L\rangle)$. (*b*) Fluorescence intensity versus delay from the excitation pulse of free ANS (*dashed line*) and apomyoglobin/ANS (*solid line*), normalized to 1.

To take advantage of the simple functional expression of the ACF in Eq. 13, it is necessary to work with a large excess of ligand. But then, even though the quantum yield of free ANS is low, its contribution may be significant, and the ACF amplitude will diminish by the square of the fractional intensity. The forward and backward rate coefficients can only be determined if the fractional intensities of bound and free ANS are known. Gating of the FCS signal offers the opportunity to work with an excess of ANS without observing fluorescence from the free ligand. Both free ligand and unbound protein are invisible to the fluorescence assay, and thus the fractional intensity of the bound ANS equals 1, which simplifies the mathematical expres-

sion for the ACF, Eq. 13, to

$$G(\tau) = G_D(\tau, N_M + N_{ML}, \tau_D)\left[1 + \frac{1}{K\langle C_L\rangle}e^{-\lambda\tau}\right]. \quad (15)$$

Fig. 3 *a* shows the ACFs of the horse heart apomyoglobin/ANS sample (diffusion and reaction) and the dye-labeled myoglobin (diffusion only). The former was measured with a gate width of 2 ns and, thus, the entire free ANS contribution to the autocorrelation function was suppressed. We mention in passing that the fast processes observed on the microsecond time scale can be attributed to after pulsing of the APD. In critical applications, this effect can be removed from the data by dividing the beam in two with a beamsplitter, detecting photons in each channel separately, and cross-correlating their output signals (Widengren et al., 1994; Bonnet et al., 1998).

The diffusion part can be removed from Eq. 15 by taking the ratio of the two ACFs in Fig. 3 *a*, which leaves us with the reaction term (apart from a trivial scaling factor). This ratio is plotted in the lower panel. The step seen in the millisecond time range represents the relaxation process due to the ligand binding reaction. Note that the apomyoglobin/ANS reaction is less than ideal for FCS studies because the reaction occurs on a similar time scale as diffusion. In studies where the reaction dynamics is much faster than diffusion, a discrete step in $G(\tau)$ has been observed before the diffusive decay (Haupts et al., 1998). By fitting the ratio in Fig. 3 *a*, both the apparent rate coefficient $\lambda = 1200$ $(+1000/-540)$ s^{-1} and the equilibrium coefficient $K = 1.1$ $(+0.5/-0.3)$ μM^{-1} were determined. The latter value for horse heart apomyoglobin is similar to the one determined for ANS binding to sperm whale apomyoglobin, $K = 0.3$ μM^{-1} (Stryer, 1965).

One may argue that the pseudo-first-order condition is not well fulfilled because our experiments were done with 300 nM apomyoglobin and 1 μM ANS. However, in the nanomolar concentration range, protein adsorption to the glass walls of our sample holder is significant, and because of the large surface-to-volume ratio, only a fraction of the apomyoglobin remains in solution in equilibrium. To obtain the real concentration, we fitted the ACF, Eq. 13, to the apomyoglobin/ANS data in Fig. 3 *a* (upper panel), using the apparent rate coefficient λ, equilibrium constant K, ligand concentration $\langle C_L\rangle$, and diffusion time τ_D, but leaving the average number of protein molecules in the sample volume, $N_M + N_{ML}$, as the only free parameter. In this case, a particle number corresponding to an actual concentration of apomyoglobin of 70 nM was obtained, and hence the pseudo-first-order assumption is justified. With this protein concentration, the microscopic rate coefficients were determined as $k_f = 640$ $(+610/-330)$ $\mu M^{-1}s^{-1}$ and $k_b = 560$ $(+170/-150)$ s^{-1}.

Lifetime heterogeneity of fluorescent labels attached to biomolecules

As a third example, we discuss the application of the electronic gate to investigations of lifetime heterogeneity of fluorescently labeled biopolymers. Conventional FCS can only distinguish heterogeneous populations of species with markedly different diffusion coefficients. Using lifetime gating, however, the different species can be separated on the basis of their contribution to the amplitude of the ACF.

To demonstrate this strategy, we performed FCS measurements on sperm whale metmyoglobin and apomyoglobin, labeled with TMR either randomly or at a particular site on the protein surface. In these experiments, the gate width was set to suppress quanta within the first 2 ns from the excitation pulse. To unambiguously relate the effects of gating on the ACF to the lifetime, fluorescence decay data were also collected in parallel for all samples studied.

ACFs of stochastically labeled metmyoglobin taken with and without the gate are shown in Fig. 4 *a*. Their amplitudes

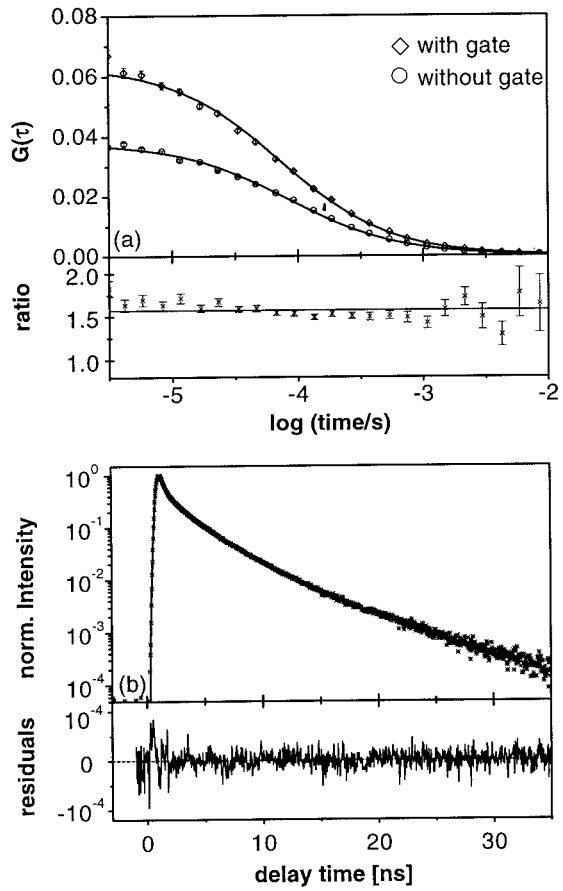

FIGURE 4 FCS and fluorescence decays of stochastically labeled sperm whale metmyoglobin. (*a*) ACFs, measured with and without gate, and the ratio of both functions in the lower panel. The solid lines are fits with Eq. 4. (*b*) Fluorescence intensity versus delay time from the excitation pulse (*points*) and fit using a four-component exponential decay (*solid line*). The residuals are plotted in the lower panel.

differ by a factor of 1.7, clearly signifying that the sample is heterogeneous. This is confirmed by the fluorescence decay in Fig. 4 *b*. Four exponentials are needed to fit the data satisfactorily. The fit parameters are given in Table 1. Gated FCS allows us to distinguish between (quasi-) static and dynamic lifetime heterogeneity. Static heterogeneity is caused either by different microenvironments of the fluorophores at different labeling sites or by conformational changes that are slow compared with the time scales covered by the ACF. Dynamic heterogeneity, by contrast, occurs if conformational changes affect the lifetimes within the time window of the measurement. In the following, we make the reasonably safe assumption that all molecules have essentially the same diffusion coefficient despite their possibly different conformations. If the heterogeneity is static, the ACF will be described by Eq. 3, with both terms of the sum having the same diffusion coefficient. If the heterogeneity is dynamic, the ACF is given by Eq. 10.

Static and dynamic heterogeneity can be distinguished by taking the ratio of a measurement made with and without the gate. The diffusion term cancels out in both cases. In the static case, one is left with a constant. In the dynamic case, the ratio is given by

$$\frac{G(\tau)_{w/}}{G(\tau)_{w/o}} = \left(\frac{1 + K(\Im_A^{w/} - \Im_B^{w/}/K)^2 e^{-\lambda\tau}}{1 + K(\Im_A^{w/o} - \Im_B^{w/o}/K)^2 e^{-\lambda\tau}}\right), \qquad (16)$$

where *w/* and *w/o* refer to the data taken with and without gate. The apparent reaction rate coefficient can be determined from a fit with this expression, and the individual components, k_f and k_b, can be calculated if the relative intensities are measured or if the equilibrium coefficient is known.

The ratio of the ACFs in Fig. 4 *a* (lower panel) is constant within error throughout the entire time window limited by the diffusion, implying that the heterogeneity is static on the 10-ms time scale. Note that an offset in one of the ACFs will change the ratio artificially at long times where the offset becomes a significant portion of the remaining correlation signal. Consequently, it is important that there are no long-term drifts or fluctuations from large aggregates that keep the correlation function from decaying to zero.

For this randomly labeled metmyoglobin sample, a distribution of fluorescence lifetimes is expected because of distance-dependent quenching by the heme group. TMR fluorophores attached to a lysine in the vicinity of the heme group should experience significant quenching, whereas those further away may exhibit lifetimes similar to those of free TMR in solution. Longer lifetimes are also observed, possibly due to steric hindrances of the bound dye. To investigate the role of the heme group in causing lifetime heterogeneity, we have performed the same experiments with stochastically labeled apomyoglobin. Figure 5 *a* shows ACFs measured with and without gate; the corresponding fluorescence decays are shown in Fig. 5 *b*. The ratio of the ACF amplitudes measured with and without the gate is 1.3, much less than for the previous sample. Consistently, the reduced curvature of the lifetime decay indicates less het-

TABLE 1 Parameters from least-squares fits of exponentials to the fluorescence decay of TMR-labeled sperm whale myoglobin

Sample	Relative amplitude	Lifetime (ns)	Reduced χ^2
metmyoglobin	0.65	0.15	
	0.17	0.80	
	0.16	2.62	
	0.02	6.17	1.3
apomyoglobin	0.13	0.36	
	0.64	2.13	
	0.23	3.72	1.4
met-E109C	0.47	0.49	
	0.51	1.18	
	0.02	4.27	1.4
apo-E109C	0.68	2.51	
	0.32	4.13	1.2

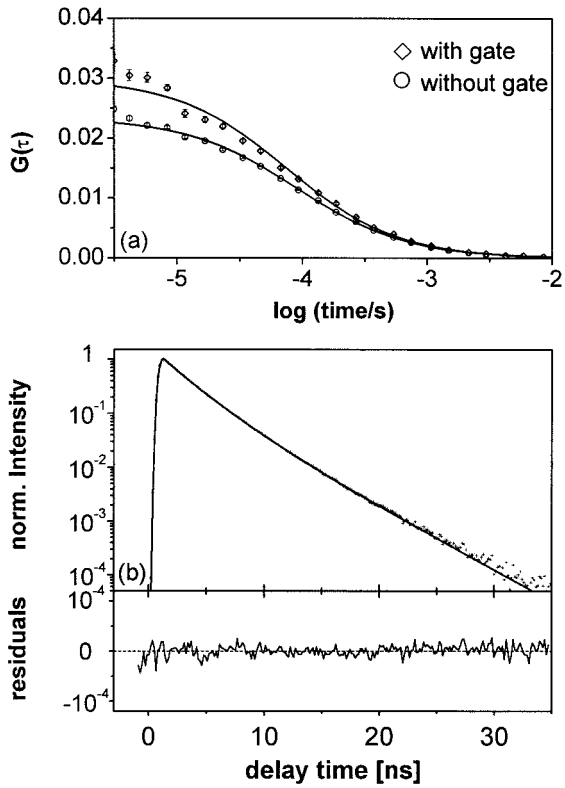

FIGURE 5 FCS and fluorescence decays of stochastically labeled sperm whale apomyoglobin: (*a*) ACFs, measured with and without gate. The solid lines are fits with Eq. 4. (*b*) Fluorescence intensity versus delay time from the laser pulse (*points*) and fit using a three-component exponential decay (*solid line*). The residuals are plotted in the lower panel.

erogeneity. Indeed, the short lifetime components in Table 1 are much weaker, and a satisfactory fit is obtained with only three exponentials. However, from both the amplitude change and the fluorescence decay it is obvious that the heme group is not entirely responsible for the lifetime heterogeneity of the sample.

The random labeling could be a potential reason for the observed static heterogeneity. To assess the contribution of site heterogeneity, the same experiment was performed with a mutant, which allowed for specific labeling of the thiol side chain of C109 with TMR. For the heme-containing met form, ACFs measured with and without the gate are plotted in Fig. 6 *a* and the fluorescence decay in Fig. 6 *b*. Measurements on specifically labeled apomyoglobin were also performed, with results consistent with those for stochastically labeled apomyoglobin and are not shown here. Fit parameters for specifically labeled metmyoglobin and apomyoglobin are included in Table 1.

From the dominance of the short lifetime components in the fluorescence decay and the factor 3.4 change in amplitude of the ACF upon gating, it is evident that specifically labeled metmyoglobin still has a large degree of heterogeneity. Thus, the coupling to the heme group varies greatly when TMR is bound to a specific site. This effect is much larger than the heterogeneity between different labeling sites in the absence of the heme group. For specifically labeled apomyoglobin, we have observed a ratio of 1.1 for ACFs collected with and without gate, showing that a small effect of lifetime heterogeneity exists even without the heme group. This can be explained by assuming slightly different conformations with interconversion times slower than milliseconds that provide a different coupling between the TMR label and aromatic amino acids in its vicinity, particularly Y103 and W14.

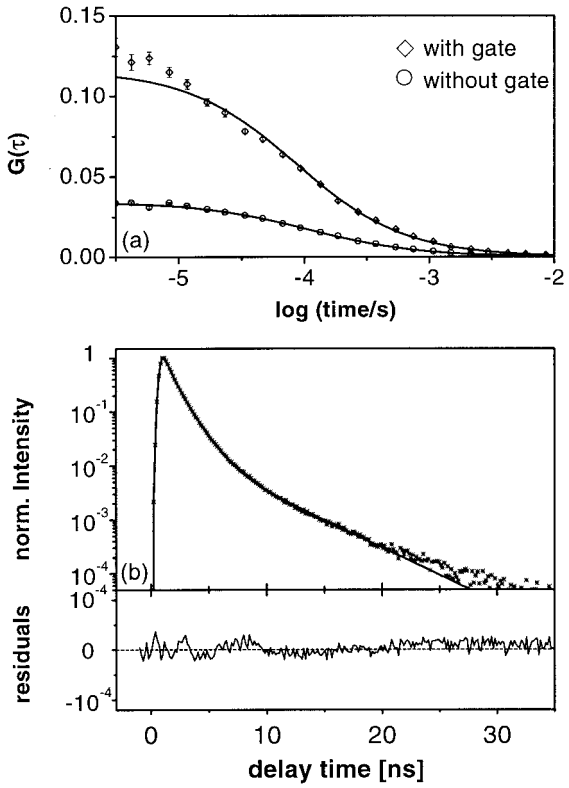

FIGURE 6 FCS and fluorescence decays of metmyoglobin mutant E109C, labeled specifically at residue 109. (*a*) ACFs, measured with and without gate. The solid lines are fits with Eq. 4. (*b*) Fluorescence intensity versus delay time from the laser pulse (*points*) and fit using a three-component exponential decay (*solid line*). The residuals are plotted in the lower panel.

CONCLUSIONS

Using pulsed laser excitation and a simple electronic circuit, contributions from particular species can be rejected from the overall fluorescence intensity, based on the delay between excitation and emission of the fluorescent species. Here we have illustrated the usefulness of this strategy with three applications: suppression of background fluorescence, simplification of FCS reaction studies, and investigation of lifetime heterogeneity of fluorescently labeled biomolecules. The ability to measure forward and backward rates of protein fluctuations in equilibrium and to distinguish between static and dynamic heterogeneity makes it a promising tool in the investigation of protein dynamics.

Time gating is a simple yet powerful extension of the FCS method that can be performed using standard FCS apparatus and data analysis. Technically more demanding is the measurement of the time of arrival of each photon with respect to both the previous photon and the excitation pulse. This approach has the advantage that no photons are rejected in the data acquisition, and multiple gate widths can be applied to the two-dimensional data set in the subsequent data analysis. This strategy has been applied by Eggeling et al. (1998) in their burst-integrated fluorescence lifetime analysis.

Finally, we want to mention briefly the possible use of polarization and/or spectral information to vary the relative intensities of the different fluorescent species. Using dispersive optics and a multichannel detector array or, much simpler, spectral filters in front of the detector, FCS data can be collected in different wavelength regions. If a molecule fluctuates between two conformations with different emission spectra, these color fluctuations can be detected by selecting the appropriate spectral band. A particularly vivid application of this strategy is the observation of conformational changes through their effect on the efficiency of fluorescence resonance energy transfer in biomolecules labeled with a donor-acceptor pair. It may also be beneficial for some applications to measure both emission delay and photon energy simultaneously.

APPENDIX

In the limit that the characteristic time of the reaction is much smaller than the diffusional correlation time, closed-form expressions can be obtained for the ACF, which are given below.

Unimolecular reaction

If the two states A and B of the unimolecular reaction have different diffusion coefficients, and the reaction occurs much faster than the difference in propagation time of the two species (i.e., $\lambda = k_f + k_b \gg |(D_A - D_B)|/w_r^2$), the ACF is given by

$$G(\tau) = G_{Diff}(\tau, N_A + N_B, \tau_{D^+}) + G_{Diff}(\tau, N_A + N_B, \tau_{D^-})K\left(\Im_A - \frac{\Im_B}{K}\right)^2 e^{-\lambda\tau}, \quad \text{(A1)}$$

with

$$D^+ = \frac{D_A\langle C_A\rangle + D_B\langle C_B\rangle}{\langle C_A\rangle + \langle C_B\rangle} \quad \text{(A2)}$$

and

$$D^- = \frac{D_A\langle C_B\rangle + D_B\langle C_A\rangle}{\langle C_A\rangle + \langle C_B\rangle}. \quad \text{(A3)}$$

D^+ represents the average diffusion coefficient of the molecule. The form of Eq. A1 is similar to that of Eq. 10. If the reaction occurs much faster than the diffusion time of either state through the probe volume, (i.e., $\lambda \gg D_A/w_r^2, D_B/w_r^2$), the relaxation term will decay before there is much change in the amplitude of the diffusion ACF. Hence, only the amplitude of $G_{Diff}(\tau, N_A + N_B, \tau_{D^-})$ is important which is equal to the amplitude of $G_{Diff}(\tau, N_A + N_B, \tau_{D^+})$. In this case, Eq. A1 reduces to Eq. 10, where D has been replaced with D^+.

Bimolecular reaction

If the ligand is not in excess, ligand diffusion plays an important role in the reaction rate. Here we consider reactions where the diffusion of the macromolecule is not affected by the binding of the ligand and the diffusion of the ligand is much greater than the diffusion of the macromolecule (i.e., $D_{ML} = D_M \ll D_L$). For reaction correlation times much faster than diffusion time of ligands through the volume (i.e., $\lambda = k_f(\langle C_M\rangle + \langle C_L\rangle) + k_b \gg D_L/w_r^2$), the autocorrelation function is given by

$$G(\tau) = G_{Diff}(\tau, N_M + N_{ML}, \tau_D)(\Im_M + \Im_{ML})^2 + \frac{G_{Diff}(\tau,1,\tau_{D^+})}{\lambda}\left[\frac{\langle C_{ML}\rangle}{\langle C_M\rangle}\frac{k_f\langle C_M\rangle}{\langle N_M + N_{ML}\rangle}\cdot\left(\Im_M - \Im_{ML}\frac{\langle C_M\rangle}{\langle C_{ML}\rangle}\right)^2 - \frac{k_f\langle C_M\rangle}{\langle N_M\rangle}\Im_L\left(\Im_M - \Im_{ML}\frac{\langle C_M\rangle}{\langle C_{ML}\rangle}\right) + \frac{(k_f\langle C_L\rangle + k_b)}{\langle N_L\rangle}(\Im_L)^2\right] + \frac{G_{Diff}(\tau,1,\tau_{D^-})}{\lambda}\left[\frac{\langle C_{ML}\rangle}{\langle C_M\rangle}\frac{(k_f\langle C_L\rangle + k_b)}{\langle N_M + N_{ML}\rangle}\cdot\left(\Im_M - \Im_{ML}\frac{\langle C_M\rangle}{\langle C_{ML}\rangle}\right)^2 + \frac{k_f\langle C_M\rangle}{\langle N_M\rangle}\Im_L\left(\Im_M - \Im_{ML}\frac{\langle C_M\rangle}{\langle C_{ML}\rangle}\right) + \frac{k_f\langle C_M\rangle}{\langle N_L\rangle}(\Im_L)^2\right]e^{-\lambda\tau} \quad \text{(A4)}$$

where

$$D^+ = \left[D_L\frac{\langle C_L\rangle}{\langle C_L\rangle + \langle C_{ML}\rangle f} + D_M\frac{\langle C_{ML}\rangle f}{\langle C_L\rangle + \langle C_{ML}\rangle f}\right], \quad \text{(A5)}$$

$$D^- = \left[D_L\frac{\langle C_{ML}\rangle f}{\langle C_L\rangle + \langle C_{ML}\rangle f} + D_M\frac{\langle C_L\rangle}{\langle C_L\rangle + \langle C_{ML}\rangle f}\right], \quad \text{(A6)}$$

and

$$f = \frac{\langle C_M\rangle}{\langle C_M\rangle + \langle C_{ML}\rangle} \quad \text{(A7)}$$

is the fraction of macromolecules without a ligand. The ACF consists of three terms. The first represents diffusion of the macromolecule, the second diffusion of the ligand, slowed by its interaction with the macromolecule, and the third can be visualized as diffusion of a vacant binding site ("hole").

We thank Karin Nienhaus and Uwe Theilen for help with the sample preparations, Prof. Steve Sligar (UIUC) for providing the mutant plasmid, Prof. Mike Weissman (UIUC) and Prof. Enrico Gratton (UIUC) for fruitful discussions and comments regarding this manuscript. D. C. Lamb thanks the University of Ulm for a travel grant. Support from the Deutsche Forschungsgemeinschaft (grants NI-291/3-1 and Graduiertenkolleg 328) is also gratefully acknowledged.

REFERENCES

Aragón, S. R., and R. Pecora. 1976. Fluorescence correlation spectroscopy as a probe of molecular dynamics. *J. Chem. Phys.* 64:1791–1803.

Antonini, E., and M. Brunori. 1971. Hemoglobin and Myoglobin in Their Reactions with Ligands. North-Holland, Amsterdam.

Bismuto, E., E. Gratton, I. Sirangelo, and G. Irace. 1993. Structure and dynamics of the acidic compact state of apomyoglobin by frequency-domain fluorometry. *Eur. J. Biochem.* 218:213–219.

Bismuto, E., G. Irace, I. Sirangelo, and E. Gratton. 1996. Pressure-induced perturbation of ANS-apomyoglobin complex: frequency domain fluorescence studies on native and acidic compact states. *Protein Sci.* 5:121–126.

Bonnet, G., O. Krichevsky, and A. Libchaber. 1998. Kinetics of conformational fluctuations in DNA hairpin-loops. *Proc. Natl. Acad. Sci. USA.* 95:8602–8606.

Chen, Y., J. D. Müller, P. T. C. So, and E. Gratton. 1999. The photon counting histogram in fluorescence fluctuation spectroscopy. *Biophys. J.* 77:553–567.

Eggeling, C., J. R. Fries, L. Brand, R. Günther, and C. A. M. Seidel. 1998. Monitoring conformational dynamics of a single molecule by selective fluorescence spectroscopy. *Proc. Natl. Acad. Sci. USA.* 95:1556–1561.

Ehrenberg, M., and R. Rigler. 1974. Rotational Brownian motion and fluorescence intensity fluctuations. *Chem. Phys.* 4:390–401.

Eigen, M., and R. Rigler. 1994. Sorting single molecules: application to diagnostics and evolutionary biotechnology. *Proc. Natl. Acad. Sci. USA.* 91:5740–5747.

Elson, E. L., and D. Magde. 1974. Fluorescence correlation spectroscopy. I. Conceptual basis and theory. *Biopolymers.* 13:1–27.

Göppert-Mayer, M. 1931. Über Elementarakte mit zwei Quantensprüngen. *Ann. Phys.* 9:273–294.

Haupts, U., S. Maiti, P. Schwille, and W. W. Webb. 1998. Dynamics of fluorescence fluctuations in green fluorescent protein observed by fluorescence correlation spectroscopy. *Proc. Natl. Acad. Sci. USA.* 95: 13573–13578.

Kask, P., P. Piksarv, M. Pooga, Ü. Mets, and E. Lippmaa. 1989. Separation of the rotational contribution in fluorescence correlation experiments. *Biophys. J.* 55:213–220.

Kask, P., K. Palo, D. Ullmann, and K. Gall. 1999. Fluorescence-intensity distribution analysis and its application in biomolecular detection technology. *Proc. Natl. Acad. Sci. USA.* 24:13756–13761.

Kettling, U., A. Koltermann, P. Schwille, and M. Eigen. 1998. Real-time enzyme kinetics monitored by dual-color fluorescence cross-correlation spectroscopy. *Proc. Natl. Acad. Sci. USA.* 95:1416–1420.

Koppel, D. E. 1974. Statistical accuracy in fluorescence correlation spectroscopy. *Phys. Rev. A.* 10:1938–1945.

Magde, D., E. L. Elson, and W. W. Webb. 1974. Fluorescence correlation spectroscopy. II. An experimental realization. *Biopolymers.* 13:29–61.

Magde, D. 1976. Chemical kinetics and fluorescence correlation spectroscopy. *Quart. Rev. Biophys.* 9:35–47.

Maiti, S., U. Haupts, and W. W. Webb. 1997. Fluorescence correlation spectroscopy: diagnostics for sparse molecules. *Proc. Natl. Acad. Sci. USA.* 94:11753–11757.

Palmer III, A. G., and N. L. Thompson. 1989. Intensity dependence of high-order autocorrelation functions in fluorescence correlation spectroscopy. *Rev. Sci. Instrum.* 60:624–633.

Rauer, B., E. Neumann, J. Widengren, and R. Rigler. 1996. Fluorescence correlation spectrometry of the interaction kinetics of tetramethylrhodamin α-bungarotoxin with *Torpedo californica* acetylcholine receptor. *Biophys. Chem.* 58:3–12.

Schwille, P., J. Bieschke, and F. Oehlenschäger. 1997. Kinetic investigations by fluorescence correlation spectroscopy: the analytical and diagnostic potential of diffusion studies. *Biophys. Chem.* 66:211–228.

Sirangelo, I., E. Bismuto, S. Tavassi, and G. Irace. 1998. Apomyoglobin folding intermediates characterized by the hydrophobic fluorescent probe 8-anilino-1-naphthalene sulfonate (ANS). *Biochim. Biophys. Acta.* 1385:69–77.

Springer, B. A., and S. G. Sligar. 1987. High-level expression of sperm whale myoglobin in *Escherichia coli. Proc. Natl. Acad. Sci. USA.* 84:8961–8965.

Stryer, L. 1965. The interaction of a naphthalene dye with apomyoglobin and apohemoglobin: a fluorescent probe of non-polar binding sites. *J. Mol. Biol.* 13:482–495.

Teale, F. W. J. 1959. Cleavage of the haem-protein link by acid methylethylketone. *Biochim. Biophys. Acta.* 35:543.

Thompson, N. L. 1991. Fluorescence correlation spectroscopy. *In* Topics in Fluorescence Spectroscopy, Volume 1: Techniques. J. R. Lakowicz, editor. Plenum Press, New York. 337–378.

Widengren, J., R. Rigler, and Ü. Mets. 1994. Triplet-state monitoring by fluorescence correlation spectroscopy. *J. Fluoresc.* 4:255–258.

Widengren, J., Ü. Mets, and R. Rigler. 1995. Fluorescence correlation spectroscopy of triplet states in solution: a theoretical and experimental study. *J. Phys. Chem.* 99:13368–13379.